

Multi-Representation Diagrams for Pain Recognition: Integrating Various Electrodermal Activity Signals into a Single Image

Stefanos Gkikas
gkikas@ics.forth.gr
Foundation for Research &
Technology-Hellas
Heraklion, Greece

Ioannis Kyprakis
ikyprakis@ics.forth.gr
Foundation for Research &
Technology-Hellas
Heraklion, Greece

Manolis Tsiknakis
tsiknaki@ics.forth.gr
Foundation for Research &
Technology-Hellas and Hellenic
Mediterranean University
Heraklion, Greece

Abstract

Pain is a multifaceted phenomenon that affects a substantial portion of the population. Reliable and consistent evaluation benefits those experiencing pain and underpins the development of effective and advanced management strategies. Automatic pain-assessment systems deliver continuous monitoring, inform clinical decision-making, and aim to reduce distress while preventing functional decline. By incorporating physiological signals, these systems provide objective, accurate insights into an individual's condition. This study has been submitted to the *Second Multimodal Sensing Grand Challenge for Next-Gen Pain Assessment (AI4PAIN)*. The proposed method introduces a pipeline that leverages electrodermal activity signals as input modality. Multiple representations of the signal are created and visualized as waveforms, and they are jointly visualized within a single multi-representation diagram. Extensive experiments incorporating various processing and filtering techniques, along with multiple representation combinations, demonstrate the effectiveness of the proposed approach. It consistently yields comparable, and in several cases superior, results to traditional fusion methods, establishing it as a robust alternative for integrating different signal representations or modalities.

CCS Concepts

• **Applied computing** → **Health informatics**.

Keywords

Pain assessment, EDA, deep learning, data fusion

ACM Reference Format:

Stefanos Gkikas, Ioannis Kyprakis, and Manolis Tsiknakis. 2025. Multi-Representation Diagrams for Pain Recognition: Integrating Various Electrodermal Activity Signals into a Single Image. In *Proceedings of October 13–17, 2025 (ICMI)*. ACM, New York, NY, USA, 10 pages. <https://doi.org/XXXXXXX.XXXXXXX>

Permission to make digital or hard copies of all or part of this work for personal or classroom use is granted without fee provided that copies are not made or distributed for profit or commercial advantage and that copies bear this notice and the full citation on the first page. Copyrights for components of this work owned by others than the author(s) must be honored. Abstracting with credit is permitted. To copy otherwise, or republish, to post on servers or to redistribute to lists, requires prior specific permission and/or a fee. Request permissions from permissions@acm.org.
ICMI,

© 2025 Copyright held by the owner/author(s). Publication rights licensed to ACM.
ACM ISBN 978-x-xxxx-xxxx-x/YYYY/MM
<https://doi.org/XXXXXXX.XXXXXXX>

1 Introduction

Pain serves as a vital evolutionary mechanism, alerting the organism to potential harm or signaling the onset of illness. It plays a critical role in the body's defense system by helping preserve physiological integrity [53]. According to the biopsychosocial model, pain is not merely a physical sensation but the result of complex interactions among biological, psychological, and social factors [7]. Pain has been described as a "*Silent Public Health Epidemic*" [30], emphasizing its widespread yet often underestimated impact. In nursing literature, it is also referred to as "*the fifth vital sign*" [29], reflecting the need for its routine and systematic assessment alongside other vital signs. In the U.S., an estimated 50 million people suffer daily from acute, chronic, or end-of-life pain, making it the leading reason for emergency room visits and medical consultations [57]. In addition, the widespread misuse of and addiction to pain medications have driven the opioid crisis in the United States, imposing substantial medical and social costs and causing numerous fatalities [39]. In 2017 alone, opioid overdoses resulted in nearly 47,000 fatalities [61].

The inherent subjectivity and complexity of pain assessment have been identified as significant challenges in both research and clinical practice. For example, pain management often relies on patients' subjective reports, making it difficult to administer medication with precision. This lack of objective evaluation contributes significantly to the overprescription and overuse of pain medications [36]. Moreover, managing and assessing pain in patients with—or at risk of—medical instability presents significant clinical challenges, particularly when communication barriers are present [50]. Research highlights that pain in critically ill adults remains frequently under-managed. A significant limitation is the lack of structured, comprehensive tools for assessing pain and supporting clinical decision-making in these contexts [40]. Furthermore, cancer-related pain is highly prevalent, especially during advanced disease stages, where its occurrence exceeds 40% [2].

Pain assessment strategies span a broad spectrum. Self-reporting methods, including numerical rating scales and questionnaires, remain the gold standard for assessing patient experiences. In parallel, behavioral indicators—such as facial expressions, vocalizations, and body movements—are also used to infer pain, particularly in non-communicative patients [9]. Physiological measures, such as electrocardiography (ECG), electromyography (EMG), and electrodermal activity (EDA), further enhance assessment by providing objective insights into the body's response to pain [21]. Electrodermal phenomena are primarily regulated by regions of the central nervous system involved in the classical sympathetic activation of

sweat secretion. Nonetheless, a range of subcortical and cortical areas also contribute to the complex mechanisms governing EDA [5]. EDA captures changes in skin conductivity, which reflect sweat gland activity, and is widely regarded as a noninvasive indicator of sympathetic nervous system function. As such, it has gained prominence as a valuable physiomaer in both clinical and non-clinical contexts for evaluating SNS dynamics [36]. Electrodermal activity has long been recognized as a reliable index for quantifying emotional responses [56], stress-related arousal [41], and stress [35]. In the domain of pain-related clinical applications, EDA is frequently utilized to evaluate the analgesic impact of treatments, therapies, or pharmacological interventions. For instance, [45] reported a significant decrease in EDA integral values during therapy for low back pain, which corresponded with reduced pain intensity.

This study explores the application of electrodermal activity (EDA) as a standalone modality within an automatic pain assessment pipeline. Although prior research has demonstrated the relevance of EDA in pain assessment and introduced various methods for processing, filtering, and modeling, the proposed pipeline integrates the most effective aspects of these approaches. It introduces a parallel processing scheme that creates multiple representations of the original EDA signal. These representations are visualized as waveforms and fused into multi-representation diagrams, resulting in a multimodal-inspired framework based entirely on a single modality—EDA.

2 Related Work

Over the past 15 years, interest in automatic pain assessment has steadily increased, with developments progressing from classical image and signal processing techniques to more advanced deep learning-based approaches [14]. The majority of existing methods are video-based, aiming to capture behavioral cues through facial expressions, body movements, or other visual indicators and employing a wide range of modeling strategies [3, 22, 23, 25]. While video-based approaches dominate the field, a considerable number of studies have also focused on biosignal-based methods, although to a lesser extent. These works have investigated the utility of various physiological signals, such as electrocardiography (ECG) [15, 16], electromyography (EMG) [43, 44, 55, 60], and brain activity through functional near-infrared spectroscopy (fNIRS) [12, 13, 33, 51, 52]. In addition, multimodal approaches combining behavioral and physiological data have gained increasing attention in recent years, with several studies demonstrating the benefits of integrating multiple sources of information to improve performance [8, 19, 20, 27, 28, 62]. For a comprehensive overview of methods employed in automatic pain recognition frameworks, refer to [21, 32].

Several studies have employed EDA signals for automatic pain assessment, spanning classical signal processing and feature engineering pipelines as well as deep-learning frameworks. For example, Aziz *et al.* [1] used time-, spectral-, and cepstral-domain representations of EDA to extract features and trained several conventional classifiers. The authors in [26] derived features from the frequency, time, and wavelet domains and employed ordinal-regression neural networks. Interestingly, the study in [54] analyzed both tonic and phasic EDA components, generating an extensive set of handcrafted features to compare electrical and pressure stimuli for pain

recognition. The authors in [47] utilized phasic EDA components and developed a hybrid 1D model combining temporal convolutional networks with long short-term memory (LSTM) networks, achieving strong pain-detection performance. In [37], temporal convolution and cross-attention networks, together with multiscale time windows, delivered high pain-assessment accuracy. Similarly, Lu *et al.* [38] integrated squeeze-and-excitation residual networks with transformers and, through multiscale convolutional neural networks, exploited long, medium, and short temporal windows. Finally, [46] combined convolutional layers, BiLSTMs, and attention mechanisms, attaining state-of-the-art performance on benchmark datasets.

3 Methodology

This section outlines the signal pre-processing steps, the creation of multi-representation diagrams, and the architecture of the proposed model. It also provides details on the augmentation and regularization techniques used.

3.1 Signal Pre-processing & Feature Extraction

Initially, the raw EDA signals $x(t)$ were low-pass filtered using a fourth-order Butterworth filter with a cutoff frequency of 5 Hz and then linearly detrended to eliminate baseline drift [10]. The resulting filtered signal $x_{\text{filt}}(t)$ was subsequently decomposed into tonic and phasic components using complementary 0.05 Hz Butterworth low- and high-pass filters [34], defined as:

$$x_{\text{tonic}}(t) = \mathcal{L}_{0.05}\{x_{\text{filt}}(t)\}, \quad x_{\text{phasic}}(t) = x_{\text{filt}}(t) - x_{\text{tonic}}(t). \quad (1)$$

The tonic component captures slow sympathetic tone, whereas the phasic component isolates rapid skin-conductance responses (SCRs). Subsequently, residual drift in the phasic component was removed through linear detrending, resulting in a zero-baseline phasic waveform $x_{\text{pd}}(t)$, computed as:

$$x_{\text{pd}}(t) = x_{\text{phasic}}(t) - \text{mean}(x_{\text{phasic}}(t)). \quad (2)$$

To calculate the time-varying sympathetic index (TVSymp), $x_{\text{pd}}(t)$ was downsampled and analysed using Variable-Frequency Complex Demodulation (VFCDM) [48, 59]. Signal components within the 0.08–0.24 Hz band—closely associated with sympathetic activation—were isolated, and their analytic amplitude was extracted using the Hilbert transform:

$$\text{TVSymp}(t) = \frac{\left| \mathcal{H} \left\{ \mathcal{B}_{0.08-0.24} \left(\text{VFCDM}(x_{\text{pd}}(t)) \right) \right\} \right|}{\sigma}, \quad (3)$$

where σ denotes the standard deviation of the resulting envelope. The resulting waveform $\text{TVSymp}(t)$ serves as a dynamic index of sympathetic nervous system activity. Lastly, a series of handcrafted features were extracted from the EDA signal to capture both temporal and spectral characteristics associated with sympathetic activity. Skin conductance responses (SCRs) were identified as local peaks in the phasic signal with amplitude $\geq 40\%$ of the dynamic range and inter-peak interval ≥ 0.5 s [4, 6], yielding features such as SCR count, amplitude statistics, inter-peak intervals, and rise-time measures. In addition, time-scale decomposition (TSD) features were computed over sliding windows of 1, 2, 4, 5, 8, and 10 s with 50% overlap. For each window length w and statistic f (mean, standard

deviation, slope, AUC, skewness, kurtosis), both the average and maximum values were calculated as:

$$\bar{f}_w = \frac{1}{K_w} \sum_{k=1}^{K_w} f_{k,w}, \quad f_w^{\max} = \max_{1 \leq k \leq K_w} f_{k,w}, \quad (4)$$

where \bar{f}_w the average of the statistic f over all K_w windows of length w , and f_w^{\max} the maximum value of that statistic across those same windows. Spectral descriptors were also derived using Welch’s method, including relative power in very-low (0–0.045 Hz), low (0.045–0.15 Hz), and high (0.15–0.4 Hz) frequency bands, along with spectral entropy and centroid. Finally, distributional properties of the filtered signal were captured by extracting the 10th, 25th, 75th, and 90th percentiles. The handcrafted feature engineering process resulted in a feature vector of length $l = 98$.

3.2 Multi-representation Diagrams

The process described in 3.1, along with the original raw signal, resulted in six distinct representations of EDA: (1) *EDA-raw*, (2) *EDA-phasic*, (3) *EDA-tonic*, (4) *EDA-detrend*, (5) *EDA-TVSymp*, and (6) *handcrafted features*. These representations were subsequently visualized as waveform diagrams. A waveform diagram illustrates the temporal evolution of a signal, capturing its amplitude, frequency, and phase characteristics. It provides a simple visualization method, avoiding the need for transformations or complex computations such as those required for spectrograms, scalograms, or recurrence plots [24]. Although the handcrafted feature vector is not a signal, it can still be visualized in the same way, as any 1D vector can be plotted in a 2D space. Each individual waveform diagram was then combined to form a multi-representation diagram with a resolution of 224×224 pixels. Figure 1 presents the individual waveform representations, while Figure 2 illustrates the combined multi-representation diagram.

3.3 Encoder

The multi-representation diagrams are processed by a hierarchical Vision Transformer encoder, pretrained on approximately 11 million images [19], which produces embeddings for the final pain classification. Each diagram is divided into non-overlapping 16×16 patches, linearly projected to $d = 768$ tokens with positional encodings, and fused through alternating spectral-mixing and self-attention blocks. The encoder architecture integrates two core components: spectral layers and self-attention layers. In the spectral layer, input tokens $x \in \mathbb{R}^{h \times w \times d}$ —where h , w , and d denote the height, width, and channel dimension, respectively—are first transformed into the frequency domain using a two-dimensional Fast Fourier Transform (FFT), resulting in a complex tensor $X = \mathcal{F}[x] \in \mathbb{C}^{h \times w \times d}$. A learnable complex filter K is then applied element-wise ($\tilde{X} = K \odot X$) to modulate the frequency components. This modulated spectrum is transformed back to the spatial domain using an inverse FFT ($x \leftarrow \mathcal{F}^{-1}[\tilde{X}]$). The output is then passed through a channel-mixing MLP defined as $\Phi(x) = W_2 \cdot \text{GELU}(\text{DWConv}(W_1 \cdot x + b_1)) + b_2$, where DWConv denotes a depthwise convolution. Layer normalization is applied both before and after the FFT and IFFT operations. The self-attention layer follows the standard multi-head attention

mechanism. For input X , attention is computed as:

$$\text{Att}(X) = \text{softmax}\left(\frac{XW_q(XW_k)^T}{\sqrt{d}}\right)XW_v, \quad (5)$$

where W_q , W_k , and W_v are the query, key, and value projection matrices, respectively. The output is then passed through a feed-forward MLP: $\Phi(x) = W_2 \cdot \text{GELU}(W_1 \cdot x + b_1) + b_2$, with layer normalization applied before and after the attention mechanism. The embedding produced by the encoder is finally passed through a fully connected layer to perform the classification task of pain recognition. We note that the encoder has been fine-tuned in an end-to-end manner along with the entire pipeline. Figure 3 presents an overview of the proposed pipeline.

3.4 Augmentation Methods & Regularization

Several data augmentation techniques are applied during training. Every 224×224 multi-representation diagram undergoes a cascade of stochastic transformations. The *AugMix* method blends three randomly generated augmentation chains with the original image, shifting a mixture of contrast, colour, and geometric perturbations to the image. In addition, *TrivialAugment* applies a single randomly chosen operation with a magnitude sampled uniformly. *Centre cropping* is applied with a probability drawn from a given range, where the crop size is selected randomly and the image is resized back to its original dimensions. *Conditional Gaussian blurring* applies noise by reducing high-frequency components. Two *Cutout* masks are applied—one placing a small number of blocks, the other covering the image with a higher number, both using blocks of equal size, 32×32 . Beyond data-level augmentation, two stochastic regularizers have been utilized. A *Dropout* layer follows the encoder, with its keep probability gradually reduced linearly over training epochs:

$$p(t) = p_{\text{start}} + \frac{t}{T}(p_{\text{end}} - p_{\text{start}}), \quad 0 \leq t \leq T. \quad (6)$$

The cross-entropy loss employs a *Label-Smoothing* based on the same linear schedule, shifting from a soft target distribution toward one-hot labels. Finally, a cosine learning-rate profile with *Warmup* and *Cooldown* schedules is also employed. All stochastic choices—operation selection, magnitudes, cropping ratios, mask locations, and probability draws—are resampled independently for every image at every batch. Throughout all experiments, the batch size is fixed to 32 and the learning rate is set to $1e-4$.

4 Experimental Evaluation & Results

This study leverages the dataset released by the challenge organizers, which consists of electrodermal activity recordings from 65 participants. Data collection took place at the Human-Machine Interface Laboratory, University of Canberra, Australia, and is divided into 41 training, 12 validation, and 12 testing subjects. Pain stimulation was induced using transcutaneous electrical nerve stimulation (TENS) electrodes positioned on the inner forearm and the back of the right hand. Two pain levels were measured: pain threshold—the minimum stimulus intensity perceived as painful (low pain), and pain tolerance—the maximum intensity tolerated before becoming unbearable (high pain). The electrodermal activity sensors were attached to the left hand, with the two electrodes positioned on the proximal phalanges of the index and middle fingers. The signals

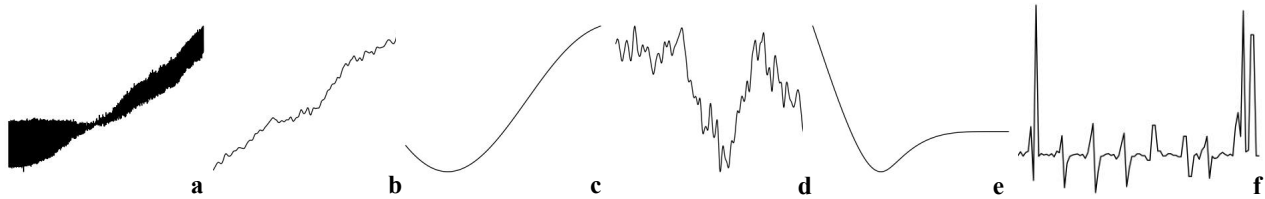


Figure 1: Waveform diagram representations: (a) EDA-raw, (b) EDA-phasic, (c) EDA-tonic, (d) EDA-detrend, (e) EDA-TVSYmp, and (f) EDA-handcrafted features.

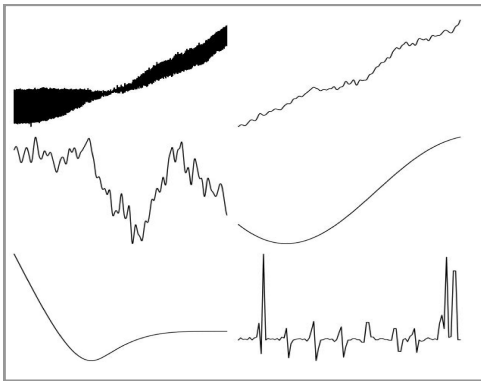


Figure 2: Multi-representation diagram composed of six waveform representations.

have a frequency of 100 Hz and a duration of approximately 10 seconds. We refer to [10] for a detailed description of the recording protocol and to [11] for information regarding the previous edition of the challenge. The experiments presented in this study are conducted on the validation subset of the dataset, evaluated under a multi-class classification framework with three levels: No Pain, Low Pain, and High Pain. The validation results are reported in terms of macro-averaged accuracy, precision, and F1 score. The final results of the testing set are also reported. We note that all experiments followed a deterministic setup, eliminating the effect of random initializations; thus, any performance differences arose strictly from the chosen optimization settings, modalities, or other intentional changes rather than chance.

4.1 Isolated Representations

In the context of representation analysis, each individual variant—namely, *EDA-raw*, *EDA-phasic*, *EDA-tonic*, *EDA-detrend*, *EDA-TVSYmp*, and *handcrafted features*—was evaluated independently as an isolated diagram. Table 1 presents the corresponding results. The first set of experiments was conducted using a training duration of 200 epochs, with the first 30 epochs utilized for warmup. We observe an accuracy of 59.73% for the raw EDA signals, while the phasic representation achieved only 46.36%, where training collapse was also observed. The detrended signals performed significantly better, achieving 71.71% accuracy, followed closely by the tonic representation at 72.07%. The highest overall performance was achieved by the final two representations: TVSYmp with 73.16%

Table 1: Comparison of performances for different EDA representations.

Epochs	Input	Schedule	Task-MC		
		Warmup	Accuracy	Precision	F1
200	Raw	30	59.73	64.17	60.69
200	Phasic	30	46.36	41.90	44.02
200	Detrend	30	71.71	72.87	72.07
200	Tonic	30	72.07	74.01	72.97
200	TVSYmp	30	73.16	75.19	73.90
200	Handcrafted	30	74.84	73.46	73.59
300	Raw	50	59.86	68.97	63.40
300	Phasic	50	54.93	57.40	56.04
300	Detrend	50	72.50	73.13	72.80
300	Tonic	50	73.28	75.01	73.80
300	TVSYmp	50	73.13	74.68	73.87
300	Handcrafted	50	74.95	73.53	74.16

MC: multiclass classification (No, Low, High Pain)

accuracy, 75.19% precision, and 73.90% F1 score, while the handcrafted features reached 74.84%, 73.46%, and 73.59% respectively. The second set of experiments extended the training duration to 300 epochs, with a 50-epoch warmup, based on the observation that the representations could benefit from longer and more stable training. While performance improved overall, the increase was not uniform across all inputs. Raw EDA saw a marginal improvement of 0.13% in accuracy. The phasic signals, however, showed the most notable gain, rising to 54.93% accuracy and avoiding the training instability observed earlier. Detrended, tonic, and handcrafted representations saw respective increases of 0.79%, 1.21%, and 0.11%, with the handcrafted features again achieving the highest accuracy at 74.95%. TVSYmp showed a modest decrease across all three metrics. Figure 4 provides a visual summary of the performance across all representations under both the 200- and 300-epoch configurations.

4.2 Fusion of Representations

The first category of fusion applied to the representations is late fusion, a classic technique. In this scheme, the encoder extracts embeddings from each individual representation, and simple operations such as addition or concatenation are employed to combine them before classification. The results are summarized in Table 2. Initially, combinations involving the raw signal and individual

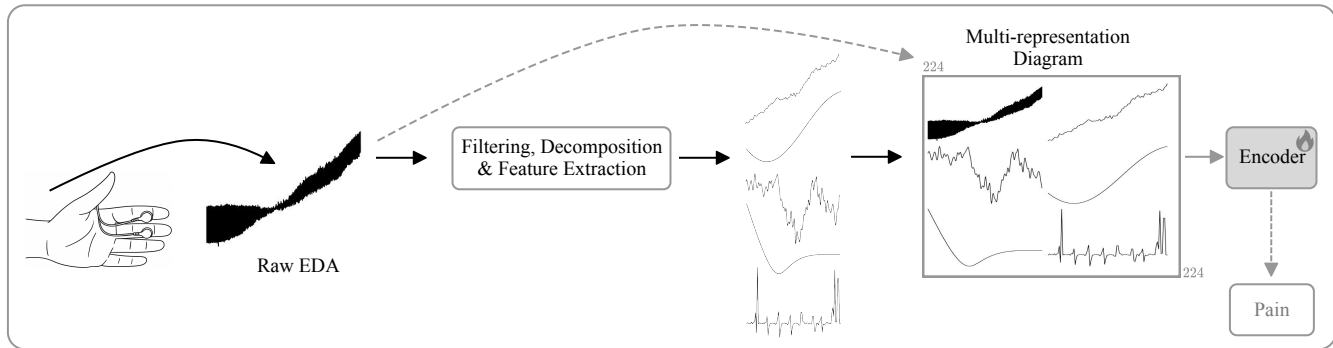


Figure 3: Schematic overview of the proposed pipeline for pain assessment using EDA signals.

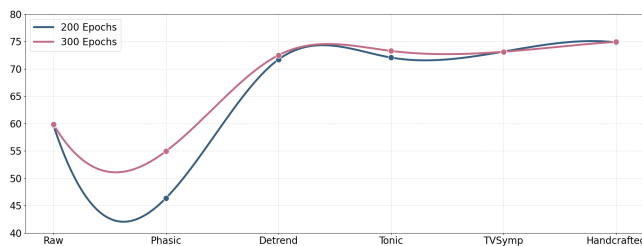


Figure 4: Visual comparison of performance across different EDA representations and training epochs.

representations were evaluated using addition. Fusion with the phasic representation yielded an accuracy of 65.50%, with detrended signals achieving 76.83%, and tonic resulted in 74.35%. Combining raw with TVSymp reached 75.86%, while raw with handcrafted features achieved 78.01%. When using concatenation for the same representation pairs, performance was generally lower on average; however, peak performance was higher. For instance, raw and detrended dropped to 71.98%, while raw and tonic increased to 78.39%. The combination of raw and handcrafted data via concatenation produced the highest overall performance in this group, with 79.49% accuracy, 80.43% precision, and 79.61% F1 score. The second group of combinations focused on the phasic representation paired with others. Using addition, phasic with detrend reached 71.98%, with tonic 74.59%, and with handcrafted 75.03%. In this group, concatenation consistently outperformed addition, with observed increases of 0.60%, 0.98%, 1.30%, and 1.54% for the phasic–detrend, phasic–tonic, phasic–TVSymp, and phasic–handcrafted pairs, respectively. The phasic–handcrafted pair with concatenation yielded the best result in this group, with 76.57% accuracy, 76.41% precision, and 76.38% F1 score. Further combinations involved three-input setups. Using addition, phasic–detrend–tonic achieved 75.50%, phasic–detrend–TVSymp 76.88%, and phasic–detrend–handcrafted 76.04%. The concatenation variant of phasic–detrend–tonic reached 78.80%, which was the highest among all three-input combinations. Other evaluated combinations included tonic–TVSymp and phasic–handcrafted. Using addition, these achieved 80.18% and 75.59%

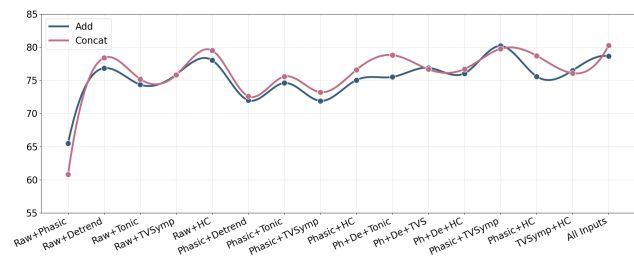


Figure 5: Visual comparison of performance across different combinations of EDA representations using the two fusion methods: addition and concatenation.

accuracy, respectively—the highest for their category. With concatenation, tonic–TVSymp experienced a slight drop, while phasic–handcrafted improved to 78.71%. In contrast, the TVSymp and handcrafted pair exhibited relatively lower performance, reaching a maximum of 76.48% via addition. Finally, combining all six available inputs yielded the best overall results. Concatenation yielded 80.27% accuracy, 81.37% precision, and 80.43% F1 score. The addition-based approach, while slightly behind in overall accuracy and F1, achieved the highest precision at 82.56%. Figure 5 provides a visual comparison of the performance across the different input combinations and fusion methods discussed above.

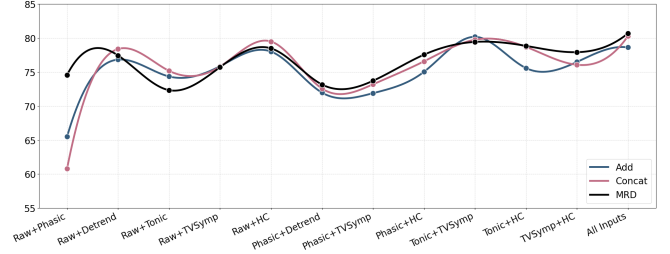
4.3 Multi-representation Diagrams

The proposed multi-representation diagrams were evaluated by combining different waveform representations, ranging from pairs to the inclusion of all six available types. Note that when only two representations are used, they are visualized vertically within the diagram, one placed above the other. The corresponding results are presented in Table 3. Visualizing the raw and phasic signals within a single diagram resulted in an accuracy of 74.58%, a substantial improvement over the classic fusion approaches, exceeding addition and concatenation by more than 9 and 13 percentage points, respectively. The raw–detrend combination reached 77.44% accuracy, outperforming the addition method, but slightly underperforming compared to concatenation. For the raw–tonic pair, an accuracy of 72.34% was recorded, approximately 2% lower than

Table 2: Comparison of performance across different EDA representation combinations and fusion methods.

Epochs	Input	Fusion	Task-MC		
			Accuracy	Precision	F1
300	Raw, Phasic	add	65.50	73.42	68.80
300	Raw, Detrend	add	76.83	78.70	77.70
300	Raw, Tonic	add	74.35	76.38	75.30
300	Raw, TVSymp	add	75.86	76.11	75.71
300	Raw, HC	add	78.01	79.09	78.44
300	Raw, Phasic	concat	60.80	61.07	60.90
300	Raw, Detrend	concat	<u>78.39</u>	<u>79.77</u>	<u>79.00</u>
300	Raw, Tonic	concat	75.18	<u>80.38</u>	77.56
300	Raw, TVSymp	concat	75.80	78.83	75.84
300	Raw, HC	concat	79.49	80.43	79.61
300	Phasic, Detrend	add	71.98	71.64	71.50
300	Phasic, Tonic	add	74.59	73.75	74.13
300	Phasic, TVSymp	add	71.89	72.64	71.43
300	Phasic, HC	add	75.03	75.64	75.33
300	Phasic, Detrend	concat	72.58	74.20	73.36
300	Phasic, Tonic	concat	<u>75.57</u>	<u>75.65</u>	<u>75.58</u>
300	Phasic, TVSymp	concat	73.19	74.58	73.76
300	Phasic, HC	concat	76.57	76.41	76.38
300	Phasic, Detrend, Tonic	add	75.50	76.62	76.03
300	Phasic, Detrend, TVSymp	add	<u>76.88</u>	77.64	<u>77.21</u>
300	Phasic, Detrend, HC	add	76.04	76.58	76.29
300	Phasic, Detrend, Tonic	concat	78.80	78.39	78.55
300	Phasic, Detrend, TVSymp	concat	76.65	<u>77.66</u>	76.32
300	Phasic, Detrend, HC	concat	76.69	76.86	74.96
300	Tonic, TVSymp	add	80.18	82.50	80.62
300	Tonic, HC	add	75.59	77.31	76.11
300	Tonic, TVSymp	concat	<u>79.75</u>	<u>79.41</u>	<u>79.38</u>
300	Tonic, HC	concat	78.71	78.76	78.69
300	TVSymp, HC	add	76.48	76.97	76.40
300	TVSymp, HC	concat	76.07	77.29	76.23
300	Raw, Phasic, Detrend, Tonic, TVSymp, HC	add	78.62	82.56	78.65
300	Raw, Phasic, Detrend, Tonic, TVSymp, HC	concat	80.27	81.37	80.43

HC: handcrafted feature diagram

**Figure 6: Visual comparison of performance across different combinations of EDA representations using the three fusion methods: addition, concatenation, and multi-representation diagrams.**

both classic fusion baselines. The raw-TVSymp fusion achieved 75.71%, closely matching the corresponding values from the standard fusion methods. Notably, combining raw and handcrafted representations yielded 78.78% accuracy, higher than addition, but slightly below concatenation. In the case of phasic and detrend, the combined diagram achieved 73.17% accuracy, improving upon the classic methods by approximately 1%. For the phasic-TVSymp pair, 73.71% was recorded, again roughly 1% higher than the baseline methods. However, the phasic-tonic combination experienced training instability, resulting in a collapse of learning and, consequently, no meaningful performance. When using the handcrafted representation with phasic, accuracy rose to 77.55%, surpassing both classic methods by approximately 1.5%. Additional combinations of detrend with tonic, TVSymp, and handcrafted representations yielded accuracies of 77.30%, 76.71%, and 76.85%, respectively. Although no direct classic fusion counterparts were available for these specific combinations, performance was consistently high. The tonic-TVSymp combination achieved 79.43% accuracy, slightly below (0.75%) the best result from concatenation. In contrast, tonic-handcrafted reached 78.85%, marginally outperforming its concatenation counterpart by 0.14%. The TVSymp-handcrafted pairing reported 77.92% accuracy, which is 1.44% higher than the best corresponding addition-based result. Finally, combining all six waveform representations within a single diagram yielded the highest overall performance: 80.67% accuracy, 81.74% precision, and 80.89% F1 score. These results exceed those obtained through the best classic fusion method (concatenation), which achieved 80.27% accuracy. Figure 6 presents a comparative overview of performance across the three fusion strategies—addition, concatenation, and the proposed multi-representation diagrams. Note that only the common representation combinations across all methods are included.

4.4 Optimization for the Multi-representation Diagrams

The final series of experiments focused on optimizing the previously reported results using the multi-representation diagrams. Prior findings had already demonstrated strong performance, particularly when all six EDA waveform representations were combined. These experiments aimed to refine the training pipeline by exploring training schedules and regularization strategies, targeting not only peak performance but also improved stability. The results are presented

Table 3: Comparison of performance across different EDA representation combinations and the proposed diagrams.

Epochs	Input	Fusion	Task-MC		
			Accuracy	Precision	F1
300	Raw, Phasic	MRD	74.58	77.08	75.53
300	Raw, Detrend	MRD	<u>77.44</u>	<u>78.26</u>	<u>77.82</u>
300	Raw, Tonic	MRD	72.34	71.35	71.79
300	Raw, TVSymp	MRD	75.71	75.77	75.69
300	Raw, HC	MRD	78.48	79.54	78.82
300	Phasic, Detrend	MRD	73.17	70.79	71.85
300	Phasic, Tonic	MRD	56.78	59.70	57.30
300	Phasic, TVSymp	MRD	<u>73.71</u>	<u>76.25</u>	<u>74.26</u>
300	Phasic, HC	MRD	77.55	77.37	77.06
300	Detrend, Tonic	MRD	77.30	76.00	76.58
300	Detrend, TVSymp	MRD	76.71	<u>76.60</u>	<u>76.59</u>
300	Detrend, HC	MRD	<u>76.85</u>	78.08	77.41
300	Tonic, TVSymp	MRD	79.43	81.13	80.22
300	Tonic, HC	MRD	78.85	78.80	78.84
300	TVSymp, HC	MRD	77.92	78.36	78.02
300	Raw, Phasic, Detrend, Tonic TVSymp, HC	MRD	80.67	81.74	80.89

MRD: multi-representation diagram

in Table 4. Initially, increasing the *Label Smoothing* probability to 30% and 70% yielded accuracies of 81.63% and 80.93%, respectively—the former showing an improvement of over 1% compared to the baseline. Applying a linear decay to the label smoothing from 70% to 10% resulted in an accuracy of 80.65%. Keeping the smoothing fixed at 70% while applying a linear decrease to *Dropout* from 90% to 10% led to 81.31%. The best performance was achieved when both *Label Smoothing* and *Dropout* were scheduled to decrease linearly, resulting in an accuracy of 82.03%. These results suggest that dynamic regularization strategies improve learning effectiveness. Subsequent experiments explored further combinations of regularization and scheduling mechanisms, such as *Warmup* and learning rate adjustments. However, these did not result in significant performance gains. Finally, it was observed that many of the earlier configurations exhibited performance spikes and fluctuations during training. To address this, a stable training schedule was implemented, where training was extended to 2000 epochs using a very low learning rate of 1×10^{-6} , along with strong regularization schedules—label smoothing decreasing from 70% to 10% and dropout from 90% to 50%. This configuration yielded an accuracy of 79.92%, with precision and F1 scores of 80.69% and 80.23%, respectively. While this was not the highest in terms of peak performance, it resulted in the smoothest and most stable training process. The training and validation curves are shown in Figure 7.

Table 4: Comparison of various optimization strategies applied to the multi-representation diagram using all six available waveform representations.

Epochs	Schedule		Regularization		Task-MC
	Warmup	LR	LS	DO	Metrics
300	50	1e-4	10-10	50-50	80.67 _[81.74 80.89]
300	50	1e-4	30-30	50-50	<u>81.63</u> _[82.56 81.41]
300	50	1e-4	70-70	50-50	80.93 _[81.00 80.92]
300	50	1e-4	70-10	50-50	80.65 _[82.08 80.42]
300	50	1e-4	70-70	90-10	81.31 _[81.88 81.00]
300	50	1e-4	70-10	70-10	82.03 _[82.14 81.90]
300	50	1e-5	70-10	50-50	79.95 _[80.48 80.15]
300	50	1e-5	70-70	90-10	79.05 _[80.39 79.58]
300	50	1e-5	70-10	70-10	78.04 _[78.81 78.25]
300	150	1e-5	70-10	50-50	79.31 _[80.25 79.70]
300	150	1e-5	70-70	90-10	79.08 _[81.58 80.25]
300	150	1e-5	70-10	70-10	79.20 _[79.97 79.35]
300	150	1e-4	70-10	50-50	79.72 _[80.06 79.56]
300	150	1e-4	70-70	90-10	80.21 _[83.43 79.70]
300	150	1e-4	70-10	70-10	80.01 _[80.88 80.39]
2000	10	1e-6	70-10	90-50	79.92 _[80.69 80.23]

Values in the format $x-y$ indicate that the corresponding parameters were linearly scheduled during training from $x\%$ to $y\%$. LR: learning rate LS: label smoothing (in %) DO: dropout rate (in %).

5 Comparison with Existing Methods

In this section, the proposed approach is compared with previous studies using the testing set of the *AI4PAIN* dataset. Some of these studies were conducted as part of the *First Multimodal Sensing Grand Challenge*. In contrast, others, including the present work, utilized data from the *Second Multimodal Sensing Grand Challenge*. The key distinction between the two challenges lies in the set of available modalities. Studies employing facial video or fNIRS have reported strong results, with accuracies of 49.00% by [49] and 55.00% by [42], respectively. Combining these two modalities also yielded competitive results, although not substantially better than using each modality alone. For instance, [58] reported 51.33%, and [19] achieved 55.69% using fused video and fNIRS data. Regarding the physiological modalities available in the *Second Grand Challenge*, some approaches achieved particularly high performance, while others showed more limited results. In [18], the authors reported 54.89% accuracy using a combination of EDA, BVP, respiration, and blood oxygen saturation (SpO₂). In contrast, [17] achieved 42.17% using only the respiration signal. The proposed method, based solely on EDA, achieved an accuracy of 55.17%—among the highest reported to date. This outcome reinforces prior findings, as EDA is widely recognized as one of the most effective modalities for pain assessment and stress-related applications, as outlined in the introduction. Table 5 presents the corresponding results and comparisons across the studies.

6 Discussion & Conclusion

This study presents our contribution to the *Second Multimodal Sensing Grand Challenge for Next-Generation Pain Assessment (AI4PAIN)*,

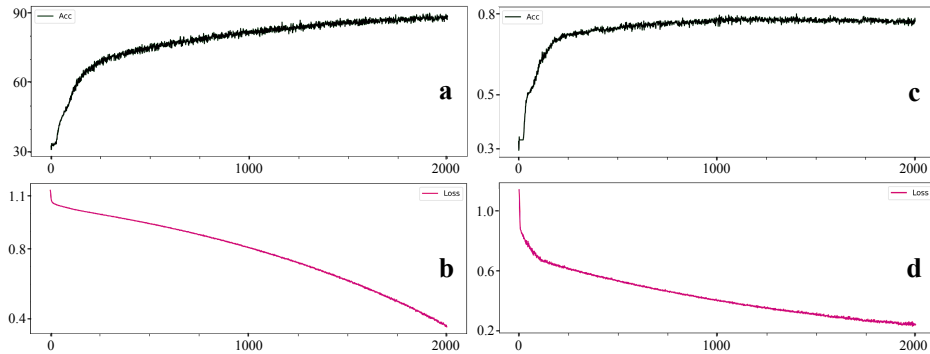


Figure 7: Visualization of the performance of the final version of the proposed method: (a) training accuracy, (b) validation accuracy, (c) training loss, and (d) validation loss.

Table 5: Comparison of studies on the testing set of the *AI4Pain* dataset.

Study	Modality	ML	Acc (%)
[31] [†]	fNIRS	ENS	53.66
[42] [†]	fNIRS	Transformer	55.00
[49] [†]	Video	2D CNN	49.00
[24] [†]	Video, fNIRS	Transformer	46.67
[58] [†]	Video, fNIRS	CNN-Transformer	51.33
[19] [†]	Video, fNIRS	Transformer	55.69
[18] [‡]	EDA, BVP, Resp, SpO ₂	MoE	54.89
[17] [‡]	Respiration	Transformer	42.24
Our [‡]	EDA	Transformer	55.17

ENS: Ensemble Classifier SpO₂: Peripheral Oxygen Saturation MoE: Mixture of Experts †: AI4PAIN-First Multimodal Sensing Grand Challenge ‡: AI4PAIN-Second Multimodal Sensing Grand Challenge

where electrodermal activity (EDA) signals were the chosen modality. A novel approach was proposed for combining different EDA signal representations into a single multi-representation diagram. This method was evaluated against classical late fusion strategies, specifically feature addition and concatenation. The results demonstrated that the proposed method achieved comparable and, in some cases, superior performance, indicating its potential as a robust alternative in scenarios requiring the integration of multiple signal representations. Additionally, the effectiveness of visualizing a smaller number of representations—either single waveforms or pairs—was also examined. These configurations showed competitive performance compared to their counterparts using traditional feature fusion or representation techniques. Overall, the findings highlight that transforming signal waveforms into image-based visualizations can be a highly effective strategy. This challenges the conventional reliance on 1D signal analysis and opens the possibility of leveraging powerful 2D vision models, which are known for their ability to extract high-quality local features. Beyond waveform visualizations, this work also explored the transformation of EDA-derived feature vectors into visual representations. These diagrams demonstrated

strong performance both independently and in combination with other inputs, suggesting the method’s applicability in feature-based approaches as well. One potential limitation of the proposed method lies in its scalability. While experiments covered up to six representations, using significantly more (*e.g.*, ten, twelve, or more) may lead to excessive compression within the diagram, which inevitably degrades performance. The challenge results confirmed the competitiveness of the proposed approach relative to other studies. This reflects the synergy between the high-performing EDA modality and the effectiveness of the multi-representation diagram approach. In conclusion, multi-representation diagrams offer a promising alternative for integrating diverse representations—whether signal-based or feature-based—particularly in settings where the total number remains moderate.

Safe and Responsible Innovation Statement

This work relied on the *AI4PAIN* dataset [10, 11], made available by the challenge organizers, to assess automatic pain recognition methods. All participants confirmed the absence of neurological or psychiatric conditions, unstable health issues, chronic pain, or regular medication use during the session. Before the experiment, participants were thoroughly informed of the procedures, and written consent was obtained. The original study’s human-subject protocol received ethical clearance from the University of Canberra’s Human Ethics Committee (*approval number: 11837*). The proposed method was developed for continuous pain monitoring, aiming to enhance pain assessment protocols and improve patient care. However, as validation and testing were performed on controlled laboratory data, its deployment in real-world clinical settings requires further investigation and comprehensive evaluation.

Acknowledgements

This work has received funding from the European Union’s Horizon 2020 research and innovation program under grant agreement No 945175 (Project: *CARDIOCARE*).

References

- [1] Sumair Aziz, Calvin Joseph, Niraj Hirachan, Luke Murtagh, Girija Chetty, Roland Goecke, and Raul Fernandez-Rojas. 2025. A two-stage architecture for identifying and locating the source of pain using novel multi-domain binary patterns of EDA.

- Biomedical Signal Processing and Control* 104 (2025), 107454. <https://doi.org/10.1016/j.bspc.2024.107454>
- [2] Yeong Hak Bang, Yoon Ho Choi, Mincheol Park, Soo-Yong Shin, and Seok Jin Kim. 2023. Clinical relevance of deep learning models in predicting the onset timing of cancer pain exacerbation. *Scientific Reports* 13, 1 (2023), 11501.
 - [3] Ghazal Bargshady, Calvin Joseph, Niraj Hirachan, Roland Goecke, and Raul Fernandez Rojas. 2024. Acute Pain Recognition from Facial Expression Videos using Vision Transformers. In *2024 46th Annual International Conference of the IEEE Engineering in Medicine and Biology Society (EMBC)*. 1–4. <https://doi.org/10.1109/EMBC53108.2024.10781616>
 - [4] Mathias Benedek and Christian Kaernbach. 2010. A continuous measure of phasic electrodermal activity. *Journal of Neuroscience Methods* 190, 1 (2010), 80–91. <https://doi.org/10.1016/j.jneumeth.2010.04.028>
 - [5] Wolfram Boucsein. 1999. Electrodermal activity as an indicator of emotional processes. *Science of Emotion and Sensibility* 2, 1 (1999), 1–25.
 - [6] Wolfram Boucsein. 2012. *Electrodermal activity*. Springer Science & Business Media.
 - [7] Steven P Cohen, Lene Vase, and William M Hooten. 2021. Chronic pain: an update on burden, best practices, and new advances. *The Lancet* 397, 10289 (2021), 2082–2097. [https://doi.org/10.1016/S0140-6736\(21\)00393-7](https://doi.org/10.1016/S0140-6736(21)00393-7)
 - [8] Jaleh Farmani, Alessandro Giuseppe, Ghazal Bargshady, and Raul Fernandez Rojas. 2025. Multimodal Automatic Acute Pain Recognition Using Facial Expressions and Physiological Signals. In *Neural Information Processing*, Mufti Mahmud, Maryam Dobarjeh, Kevin Wong, Andrew Chi Sing Leung, Zohreh Dobarjeh, and M. Tanveer (Eds.). Springer Nature Singapore, Singapore, 49–62.
 - [9] Raul Fernandez Rojas, Nicholas Brown, Gordon Waddington, and Roland Goecke. 2023. A systematic review of neurophysiological sensing for the assessment of acute pain. *NPJ Digital Medicine* 6, 1 (2023), 76. <https://doi.org/10.1038/s41746-023-00810-1>
 - [10] Raul Fernandez Rojas, Niraj Hirachan, Nicholas Brown, Gordon Waddington, Luke Murtagh, Ben Seymour, and Roland Goecke. 2023. Multimodal physiological sensing for the assessment of acute pain. *Frontiers in Pain Research* 4 (2023). <https://doi.org/10.3389/fpain.2023.1150264>
 - [11] Raul Fernandez Rojas, Niraj Hirachan, Calvin Joseph, Ben Seymour, and Roland Goecke. 2024. The AI4Pain Grand Challenge 2024: Advancing Pain Assessment with Multimodal fNIRS and Facial Video Analysis. In *2024 12th International Conference on Affective Computing and Intelligent Interaction*. IEEE.
 - [12] Raul Fernandez Rojas, Calvin Joseph, Ghazal Bargshady, and Keng-Liang Ou. 2024. Empirical comparison of deep learning models for fNIRS pain decoding. *Frontiers in Neuroinformatics* (2024). <https://doi.org/10.3389/fninf.2024.1320189>
 - [13] Raul Fernandez Rojas, Mingyu Liao, Julio Romero, Xu Huang, and Keng-Liang Ou. 2019. Cortical Network Response to Acupuncture and the Effect of the Hegu Point: An fNIRS Study. *Sensors* 19, 2 (2019). <https://doi.org/10.3390/s19020394>
 - [14] Stefanos Gkikas. 2025. A Pain Assessment Framework based on multimodal data and Deep Machine Learning methods. arXiv:2505.05396 [cs.AI] <https://arxiv.org/abs/2505.05396> arXiv preprint arXiv:2505.05396.
 - [15] Stefanos Gkikas., Chariklia Chatzaki., Elisavet Pavlidou., Foteini Verigou., Kyr- iakos Kalkanis., and Manolis Tsiknakis. 2022. Automatic Pain Intensity Estimation based on Electrocardiogram and Demographic Factors. *Proceedings of the 8th International Conference on Information and Communication Technologies for Ageing Well and e-Health - ICT4AWE*, 155–162. <https://doi.org/10.5220/0010971700003188>
 - [16] Stefanos Gkikas, Chariklia Chatzaki, and Manolis Tsiknakis. 2023. Multi-task Neural Networks for Pain Intensity Estimation Using Electrocardiogram and Demographic Factors. In *Information and Communication Technologies for Ageing Well and e-Health*. Springer Nature Switzerland, 324–337. https://doi.org/10.1007/978-3-031-37496-8_17
 - [17] Stefanos Gkikas, Ioannis Kyprakis, and Manolis Tsiknakis. 2025. Efficient Pain Recognition via Respiration Signals: A Single Cross-Attention Transformer Multi-Window Fusion Pipeline. arXiv:2507.21886 [cs.AI]
 - [18] Stefanos Gkikas, Ioannis Kyprakis, and Manolis Tsiknakis. 2025. Tiny-BioMoE: a Lightweight Embedding Model for Biosignal Analysis. arXiv:2507.21875 [cs.AI]
 - [19] Stefanos Gkikas, Raul Fernandez Rojas, and Manolis Tsiknakis. 2025. PainFormer: a Vision Foundation Model for Automatic Pain Assessment. arXiv:2505.01571 [cs.CV] <https://arxiv.org/abs/2505.01571>
 - [20] Stefanos Gkikas, Nikolaos S. Tachos, Stelios Andreadis, Vasileios C. Pezoulas, Dimitrios Zaridis, George Gkois, Anastasia Matonaki, Thanos G. Stavropoulos, and Dimitrios I. Fotiadis. 2024. Multimodal automatic assessment of acute pain through facial videos and heart rate signals utilizing transformer-based architectures. *Frontiers in Pain Research* 5 (2024). <https://doi.org/10.3389/fpain.2024.1372814>
 - [21] Stefanos Gkikas and Manolis Tsiknakis. 2023. Automatic assessment of pain based on deep learning methods: A systematic review. *Computer Methods and Programs in Biomedicine* 231 (2023), 107365. <https://doi.org/10.1016/j.cmpb.2023.107365>
 - [22] Stefanos Gkikas and Manolis Tsiknakis. 2023. A Full Transformer-based Framework for Automatic Pain Estimation using Videos. In *2023 45th Annual International Conference of the IEEE Engineering in Medicine & Biology Society (EMBC)*. 1–6. <https://doi.org/10.1109/EMBC40787.2023.10340872>
 - [23] Stefanos Gkikas and Manolis Tsiknakis. 2024. Synthetic Thermal and RGB Videos for Automatic Pain Assessment Utilizing a Vision-MLP Architecture. In *2024 12th International Conference on Affective Computing and Intelligent Interaction Workshops and Demos (ACIIW)*. 4–12. <https://doi.org/10.1109/ACIIW63320.2024.00006>
 - [24] Stefanos Gkikas and Manolis Tsiknakis. 2024. Twins-PainViT: Towards a Modality-Agnostic Vision Transformer Framework for Multimodal Automatic Pain Assessment Using Facial Videos and fNIRS. In *2024 12th International Conference on Affective Computing and Intelligent Interaction Workshops and Demos (ACIIW)*. 13–21. <https://doi.org/10.1109/ACIIW63320.2024.00007>
 - [25] Dong Huang, Xiaoyi Feng, Haixi Zhang, Zitong Yu, Jinye Peng, Guoying Zhao, and Zhaoqiang Xia. 2022. Spatio-Temporal Pain Estimation Network With Measuring Pseudo Heart Rate Gain. *IEEE Transactions on Multimedia* 24 (2022), 3300–3313. <https://doi.org/10.1109/TMM.2021.3096080>
 - [26] Xinwei Ji, Tianming Zhao, Wei Li, and Albert Zomaya. 2023. Automatic Pain Assessment with Ultra-short Electrodermal Activity Signal. In *Proceedings of the 38th ACM/SIGAPP Symposium on Applied Computing (Tallinn, Estonia) (SAC '23)*. Association for Computing Machinery, New York, NY, USA, 618–625. <https://doi.org/10.1145/3555776.3577721>
 - [27] Mingzhe Jiang, Yufei Li, Jiangshan He, Yuqiang Yang, Hui Xie, and Xueli Chen. 2024. Physiological Time-series Fusion with Hybrid Attention for Adaptive Recognition of Pain. *IEEE Journal of Biomedical and Health Informatics* (2024), 1–9. <https://doi.org/10.1109/JBHI.2024.3456441>
 - [28] Mingzhe Jiang, Riitta Rosio, Sanna Salanterä, Amir M. Rahmani, Pasi Liljeberg, Daniel S. da Silva, Victor Hugo C. de Albuquerque, and Wanqing Wu. 2024. Personalized and adaptive neural networks for pain detection from multi-modal physiological features. *Expert Systems with Applications* 235 (2024), 121082. <https://doi.org/10.1016/j.eswa.2023.121082>
 - [29] Lucille A Joel. 1999. The fifth vital sign: pain. *AJN The American Journal of Nursing* 99, 2 (1999), 9.
 - [30] Joanna G Katzman and Rollin Mac Gallagher. 2024. Pain: The Silent Public Health Epidemic. *Journal of Primary Care & Community Health* 15 (2024), 21501319241253547.
 - [31] Muhammad Umar Khan, Sumair Aziz, Luke Murtagh, Girija Chetty, Roland Goecke, and Raul Fernandez Rojas. 2025. Empirically Transformed Energy Patterns: A novel approach for capturing fNIRS signal dynamics in pain assessment. *Computers in Biology and Medicine* 192 (2025), 110300. <https://doi.org/10.1016/j.combiomed.2025.110300>
 - [32] Muhammad Umar Khan, Girija Chetty, Roland Goecke, and Raul Fernandez-Rojas. 2025. A Systematic Review of Multimodal Signal Fusion for Acute Pain Assessment Systems. *ACM Comput. Surv.* (2025). <https://doi.org/10.1145/3737281>
 - [33] Muhammad Umar Khan, Maryam Sousani, Niraj Hirachan, Calvin Joseph, Maryam Ghahramani, Girija Chetty, Roland Goecke, and Raul Fernandez-Rojas. 2024. Multilevel Pain Assessment with Functional Near-Infrared Spectroscopy: Evaluating ΔHbO₂ and ΔHHb Measures for Comprehensive Analysis. *Sensors* 24, 2 (2024). <https://doi.org/10.3390/s24020458>
 - [34] Youngho Kim, Seonggeon Pyo, Seunghee Lee, Changeon Park, and Sunghyuk Song. 2025. Estimation of Pressure Pain in the Lower Limbs Using Electrodermal Activity, Tissue Oxygen Saturation, and Heart Rate Variability. *Sensors* 25, 3 (2025). <https://doi.org/10.3390/s25030680>
 - [35] Agata Klimek, Ittay Mannheim, Gerard Schouten, Eveline J. M. Wouters, and Manon W. H. Peeters. 2025. Wearables measuring electrodermal activity to assess perceived stress in care: a scoping review. *Acta Neuropsychiatrica* 37 (2025). <https://doi.org/10.1017/neu.2023.19>
 - [36] Youngsun Kong and Ki H. Chon. 2024. Electrodermal activity in pain assessment and its clinical applications. *Applied Physics Reviews* 11, 3 (08 2024), 031316. <https://doi.org/10.1063/5.0200395>
 - [37] JiaHao Li, JinCheng Luo, YanSheng Wang, YunXiang Jiang, Xu Chen, and YuJuan Quan. 2025. Automatic Pain Assessment Based on Physiological Signals: Application of Multi-Scale Networks and Cross-Attention Cross-Attention. In *Proceedings of the 2024 13th International Conference on Bioinformatics and Biomedical Science (ICBBS '24)*. Association for Computing Machinery, New York, NY, USA, 113–122. <https://doi.org/10.1145/3704198.3704212>
 - [38] Zhenyuan Lu, Burcu Ozek, and Sagar Kamarthi. 2023. Transformer encoder with multiscale deep learning for pain classification using physiological signals. *Frontiers in Physiology* Volume 14 - 2023 (2023). <https://doi.org/10.3389/fphys.2023.1294577>
 - [39] Feijun Luo. 2021. State-level economic costs of opioid use disorder and fatal opioid overdose—United States, 2017. *MMWR. Morbidity and Mortality Weekly Report* 70 (2021).
 - [40] DA Meehan, ME McRae, DA Rourke, C Eisenring, and FA Imperial. 1995. Analgesic administration, pain intensity, and patient satisfaction in cardiac surgical patients. *American Journal of Critical Care* 4, 6 (1995), 435–442.
 - [41] Anneloes L. Meijer, Lukas P.A. Arts, Randy Gomez, and Egon L. van den Broek. 2023. Electrodermal activity: A continuous monitor of well-being. *Journal of Smart Cities and Society* 2, 4 (2023), 193–207. <https://doi.org/10.3233/SCS-230021>

- [42] Minh-Duc Nguyen, Hyung-Jeong Yang, Soo-Hyung Kim, Ji-Eun Shin, and Seung-Won Kim. 2024. Transformer with Leveraged Masked Autoencoder for video-based Pain Assessment. arXiv:2409.05088 [cs.CV]
- [43] Manisha S. Patil and Hitendra D. Patil. 2024. Ensemble Neural Networks for Multimodal Acute Pain Intensity Evaluation using Video and Physiological Signals. *Journal of Computational Analysis and Applications (JoCAAA)* 33, 05 (Sep. 2024), 779–791.
- [44] Elisavet Pavlidou and Manolis Tsiknakis. 2025. Multimodal Pain Assessment Based on Physiological Biosignals: The Impact of Demographic Factors on Perception and Sensitivity. In *Proceedings of the 11th International Conference on Information and Communication Technologies for Ageing Well and e-Health - ICT4AWE*. INSTICC, SciTePress, 320–329. <https://doi.org/10.5220/0013426800003938>
- [45] Jo Perry and Ann Green. 2018. A Longitudinal Observational Clinical Study of Neurophysiological and Patient-Reported Responses to a Program of Physiotherapy for Acute and Subacute Low Back Pain. *Journal of Manipulative and Physiological Therapeutics* 41, 6 (2018), 456–466. <https://doi.org/10.1016/j.jmpt.2017.11.003>
- [46] Kim Ngan Phan, Ngumimi Karen Iyortsuun, Sudarshan Pant, Hyung-Jeong Yang, and Soo-Hyung Kim. 2023. Pain Recognition With Physiological Signals Using Multi-Level Context Information. *IEEE Access* 11 (2023), 20114–20127. <https://doi.org/10.1109/ACCESS.2023.3248654>
- [47] Javier O. Pinzon-Arenas, Youngsun Kong, Ki H. Chon, and Hugo F. Posada-Quintero. 2023. Design and Evaluation of Deep Learning Models for Continuous Acute Pain Detection Based on Phasic Electrodermal Activity. *IEEE Journal of Biomedical and Health Informatics* 27, 9 (2023), 4250–4260. <https://doi.org/10.1109/JBHI.2023.3291955>
- [48] Hugo F. Posada-Quintero, John P. Florian, Álvaro D. Orjuela-Cañón, and Ki H. Chon. 2016. Highly sensitive index of sympathetic activity based on time-frequency spectral analysis of electrodermal activity. *American Journal of Physiology-Regulatory, Integrative and Comparative Physiology* 311, 3 (2016), R582–R591. <https://doi.org/10.1152/ajpregu.00180.2016>
- [49] Pooja Prajod, Dominik Schiller, Daksitha Withanage Don, and Elisabeth André. 2024. Faces of Experimental Pain: Transferability of Deep-Learned Heat Pain Features to Electrical Pain*. In *2024 12th International Conference on Affective Computing and Intelligent Interaction Workshops and Demos (ACIIW)*. 31–38. <https://doi.org/10.1109/ACIIW63320.2024.00009>
- [50] Kathleen A. Puntillo, Daphne Stannard, Christine Miaskowski, Karen Kehrlé, and Sheila Gleeson. 2002. Use of a pain assessment and intervention notation (P.A.I.N.) tool in critical care nursing practice: Nurses' evaluations. *Heart & Lung* 31, 4 (2002), 303–314. <https://doi.org/10.1067/mhl.2002.125652>
- [51] Raul Fernandez Rojas, Xu Huang, and Keng-Liang Ou. 2016. Region of Interest Detection and Evaluation in Functional near Infrared Spectroscopy. *Journal of Near Infrared Spectroscopy* 24, 4 (2016), 317–326. <https://doi.org/10.1255/jnirs.1239>
- [52] Raul Fernandez Rojas, Julio Romero, Jehu Lopez-Aparicio, and Keng-Liang Ou. 2021. Pain Assessment based on fNIRS using Bi-LSTM RNNs. In *2021 10th International IEEE/EMBS Conference on Neural Engineering (NER)*. 399–402. <https://doi.org/10.1109/NER49283.2021.9441384>
- [53] Vivian Santiago. 2022. Painful Truth: The Need to Re-Center Chronic Pain on the Functional Role of Pain. *Journal of Pain Research* 15 (2022), 497–512. <https://doi.org/10.2147/JPR.S347780>
- [54] Maja Sokolowska, Pawel Mruzek, Marta Biesok, and Aleksandra Badura. 2025. Towards Automatic Recognition of Pain Modality: A Pilot Study on Experimentally-Induced Pain Using Electricity and Pressure. In *Information Technology in Biomedicine*, Pawel Badura, Joanna Czajkowska, Arkadiusz Gertych, Jacek Kawa, Ewa Piętko, and Wojciech Wieclawek (Eds.). Springer Nature Switzerland, Cham, 180–193.
- [55] Patrick Thiam, Peter Bellmann, Hans A. Kestler, and Friedhelm Schwenker. 2019. Exploring deep physiological models for nociceptive pain recognition. *Sensors* 19 (10 2019), 4503. Issue 20. <https://doi.org/10.3390/s19204503>
- [56] Werner Traxel. 1960. Die Möglichkeit einer objektiven Messung der Stärke von Gefühlen. *Psychologische Forschung* 26 (1960), 75–90.
- [57] U.S. Department of Health and Human Services. 2019. Pain Management Best Practices Inter-Agency Task Force Report: Updates, Gaps, Inconsistencies, and Recommendations. <https://www.hhs.gov/sites/default/files/pmtf-final-report-2019-05-23.pdf>. Accessed June 27, 2025.
- [58] Jo Vianto, Anjitha Divakaran, Hyungjeong Yang, Soonja Yeom, Seungwon Kim, Soohyung Kim, and Jieun Shin. 2025. Multimodal Model for Automated Pain Assessment: Leveraging Video and fNIRS. *Applied Sciences* 15, 9 (2025). <https://doi.org/10.3390/app15095151>
- [59] Hengliang Wang, Kin Siu, Kihwan Ju, and Ki H Chon. 2006. A high resolution approach to estimating time-frequency spectra and their amplitudes. *Annals of biomedical engineering* 34 (2006), 326–338.
- [60] Philipp Werner, Ayoub Al-Hamadi, Robert Niese, Steffen Walter, Sascha Gruss, and Harald C. Traue. 2014. Automatic Pain Recognition from Video and Biomedical Signals. In *2014 22nd International Conference on Pattern Recognition*. 4582–4587. <https://doi.org/10.1109/ICPR.2014.784>
- [61] Nana Wilson. 2020. Drug and opioid-involved overdose deaths—United States, 2017–2018. *MMWR. Morbidity and mortality weekly report* 69 (2020).
- [62] Ruicong Zhi and Junwei Yu. 2019. Multi-modal Fusion Based Automatic Pain Assessment. In *2019 IEEE 8th Joint International Information Technology and Artificial Intelligence Conference (ITAIC)*. 1378–1382. <https://doi.org/10.1109/ITAIC.2019.8785727>